Journal of Sound and Vibration (2000) **234**(2), 311–329
doi:10.1006/jsvi.1999.2869, available online at http://www.idealibrary.com on IDEAL®

DYNAMIC ANALYSIS OF A SPUR GEAR BY THE DYNAMIC STIFFNESS METHOD

K. J. HUANG AND T. S. LIU

Department of Mechanical Engineering, National Chiao Tung University, Hsinchu 30010, *Taiwan, Republic of China*

(*Received* 15 *February* 1999, 15 *December* 1999)

This study treats a spur gear tooth as a variable cross-section Timoshenko beam to construct a dynamic model, being able to obtain transient response for spur gears of involute profiles. The dynamic responses of a single tooth and a gear pair are investigated. Firstly, polynomials are used to represent the gear blank and the tooth profile. The dynamic stiffness matrix and natural frequencies of the gear are in turn calculated. The forced response of a tooth subject to a shaft-driven transmission torque is calculated by performing modal analysis. This study takes into account time-varying stiffness and mass matrices and the gear meshing forces at moving meshing points. The forced response at arbitrary points in a gear tooth can be obtained. Calculation results of fillet stresses and strains are compared with those in the literature to verify the proposed method.

1. INTRODUCTION

With an increasing demand for high-speed machinery, the dynamic analysis for gears has become more important. Dynamic response prediction for gear teeth is a major consideration in gear design. Much literature on gear dynamics and modelling has been reviewed by Ozguven and Houser [1]. Moreover, due to high power-to-weight ratios of planetary gear trains, many papers have been presented concerning planetary gear trains [2–7].

Discrete mass–spring models are commonly utilized for dynamic analysis of gearing. The mass and stiffness matrices of gear systems were obtained by approximate models, such as single- or multi-trapezoidal and rectangular-trapezoidal beams [8–10] or plates [11]. However, gear teeth profiles generally consist of involute or other curves. Further, tooth profile modification and non-standard gear tool setting are often adopted in gear design and manufacturing. Therefore, modelling a gear tooth with straight-line profile hardly incorporated these important characteristics. Not only the stiffness of the gear tooth but the meshing position varies with time during gear meshing. In contrast to discrete models, continuous models can incorporate the varying stiffness intrinsically. However, little work on gear dynamics using continuous models has been done. Nagaya [8, 9] used taper Timoshenko beams to investigate the effects of moving speeds of dynamic loads on the deflections of gear teeth and concluded that this effect could not be neglected. Amirouche *et al.* [12] investigated teeth tip displacements and fillet strains by a model of a time and position variant external load using a finite-difference method. Vijayarangan and Ganesan [13] calculated fillet stresses by a three-dimensional finite element method incorporating damping effects.

Utilizing a dynamic stiffness method, the present work deals with dynamics of spur gears that consists of variable cross-section beams. Firstly, tooth profile formulation results from

0022-460X/00/270311 + 19 $35.00/0

a standard rack cutter profile. Secondly, a spur gear is treated as a continuum, namely Timoshenko beams fitted by some polynomials. Thirdly, the dynamic stiffness matrix of the beam is derived. Natural frequencies of the gear are in turn obtained by performing a bisection procedure. Finally, the forced responses of the gear are calculated by performing modal analysis and the Runge–Kutta method.

2. TOOTH PROFILE DESCRIPTION

Figure 1 depicts a typical spur gear whose center is at the origin of the x'–y' co-ordinate system with the x'-axis passing through the middle of the gear tooth and the y-axis through its profile bottom. This profile consists of an involute and a fillet, which are generated by a straight line and a corner on a standard rack cutter profile respectively, as shown in Figure 2. Using the equation of meshing [14], the equations of the involute part of the gear are derived as

$$x' = (\ell \cos\alpha - a_r + r_p)\cos\lambda_i - (\ell \cos\alpha - a_r \tan\alpha - b - r_p\lambda_i)\sin\lambda_i, \tag{1}$$

$$y' = (\ell \cos\alpha - a_r + r_p)\sin\lambda_i + (\ell \cos\alpha - a_r \tan\alpha - b - r_p\lambda_i)\cos\lambda_i, \tag{2}$$

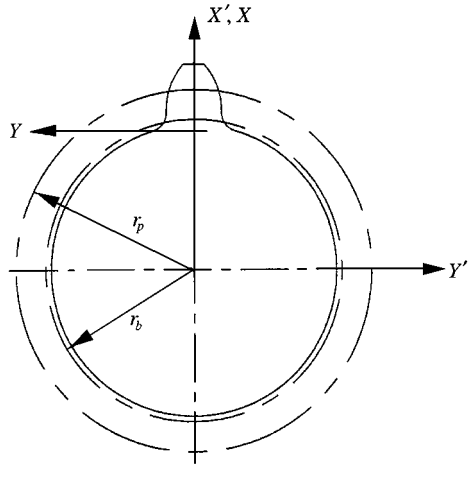

Figure 1. Co-ordinate systems of gear tooth profile including involutes and fillets.

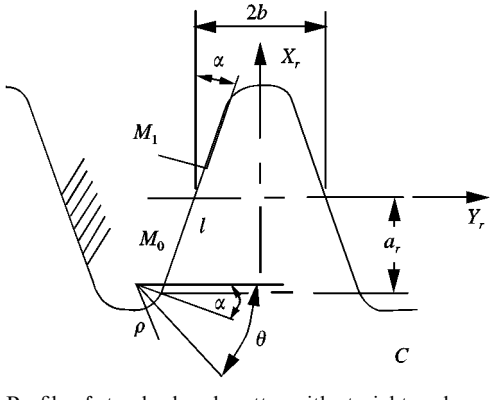

Figure 2. Profile of standard rack cutter with straight and corner parts.

where ℓ is a distance from point M_0, which is an interconnection of the straight line and the corner with a radius ρ, to an arbitrary point M_1 depicted in Figure 2, a_r the addendum coefficient, and α the pressure angle. r_p is the radius of the pitch circle, and the gear rotation angle λ_i when the involute part is generated by a cutter is written as

$$\lambda_i = \left(\ell - \frac{a_r}{\cos\alpha} - b\sin\alpha \right) \Big/ r_p \sin\alpha. \tag{3}$$

Similarly, the equations of the fillet part are derived as

$$x' = (-a_r + \rho\sin\alpha - \rho\sin\theta + r_p)\cos\lambda_f + (a_r\tan\alpha + b + \rho\cos\alpha - \rho\cos\theta + r_p\lambda_f)\sin\lambda_f, \tag{4}$$

$$y' = (-a_r + \rho\sin\alpha - \rho\sin\theta + r_p)\cos\lambda_f - (a_r\tan\alpha + b + \rho\cos\alpha - \rho\cos\theta + r_{p\lambda_f})\cos\lambda_f, \tag{5}$$

where the rotation angle λ_f during cutting the fillet part is written as

$$\lambda_f = (\rho\sin\alpha\cot\theta - \rho\cos\alpha - a_r\tan\alpha - a_r\cot\theta - b)/r_p. \tag{6}$$

The functions in equations (1)–(6), used to express the gear tooth profile, are transcendental. In this work, based on tooth profile data calculated from equations (1)–(6), polynomials will be used to represent tooth profiles to facilitate solving dynamic equations for Timoshenko beams using a power-series method presented in the next section. Only one polynomial is required for the fillet part. The involute part is firstly discretized into two elements for polynomial fitting. One of the two elements in the involute part is further divided into two elements at an instantaneous meshing point that is determined by using equations (1)–(6) of teeth profiles for the mating gears and conditions of continuous tangency [14]. During teeth meshing, due to the movement of the time-varying meshing point, the meshing point has to be recalculated for each computing time step. Each beam element is fitted by a quadratic function using a least-squares fitting. Finally, totally nine points are used to fit the four non-uniform cross-section beam elements.

3. TIMOSHENKO BEAM VIBRATION

The equations of motion for a Timoshenko beam shown in Figure 3, which account for gear tooth dynamics, will be solved to formulate dynamic stiffness matrices dealing with longitudinal and bending vibrations respectively. The gear tooth consists of some variable cross-section beam elements whose profiles are fitted by polynomials. The longitudinal displacement $u_0(x,t)$ and transverse displacement $w(x,t)$, which are functions of position variable x and time t, are written as [15]

$$u_0 = u(x,t) - y\phi(x,t), \tag{7}$$

$$w = w(x,t), \tag{8}$$

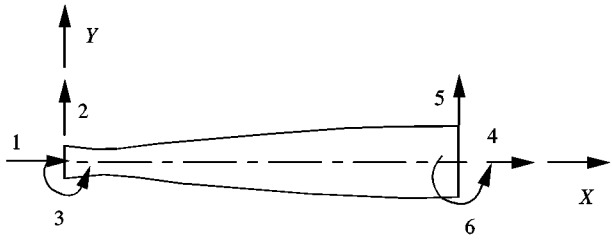

Figure 3. Typical beam element and degrees of freedom.

where $u(x,t)$ is a longitudinal displacement caused by longitudinal forces, y the transverse position variable, and $\phi(x,t)$ the bending slope. Following from linear strain–displacement relations, the normal strain ε_{xx} and shear strain ε_{xy} for the Timoshenko beam are expressed as

$$\varepsilon_{xx} = \frac{\partial u_0(x,t)}{\partial x} = \frac{\partial u(x,t)}{\partial x} - y\,\frac{\partial \phi(x,t)}{\partial x}, \tag{9}$$

$$\varepsilon_{xy} = \frac{1}{2}\left(\frac{\partial w(x,t)}{\partial x} + \frac{\partial u_0(x,t)}{\partial y}\right) = \frac{1}{2}\left(\frac{\partial w(x,t)}{\partial x} - \phi(x,t)\right), \tag{10}$$

where $\partial w(x,t)/\partial x$ represents the beam slope. Force–strain relations of the beam element including longitudinal force $B(x)$, shear force $V(x)$, and bending moment $M(x)$ are written as

$$B(x) = EA(x)\,\frac{\partial u(x)}{\partial x}, \tag{11}$$

$$V(x) = kGA(x)\left[\frac{\partial w(x)}{\partial x} - \phi(x)\right], \tag{12}$$

$$M(x) = -EI(x)\,\frac{\partial \phi(x)}{\partial x}, \tag{13}$$

where $A(x)$ is the cross-sectional area, $I(x)$ the moment of the cross-sectional area, E the Young's modulus, G the shear modulus of elasticity, and k the shear correction factor. The equations of motion for the Timoshenko beam are given as

$$-\rho A(x)\,\frac{\partial^2 u}{\partial t^2} + \frac{\partial}{\partial x}\left[EA(x)\,\frac{\partial u}{\partial x}\right] = 0, \tag{14}$$

$$-\rho A(x)\,\frac{\partial^2 w}{\partial t^2} + \frac{\partial}{\partial x}\left[kGA(x)\left(\frac{\partial w}{\partial x} - \phi\right)\right] = 0, \tag{15}$$

$$-\rho I(x)\,\frac{\partial^2 \phi}{\partial t^2} + \frac{\partial}{\partial x}\left[EI(x)\,\frac{\partial \phi}{\partial x}\right] + \left[kGA(x)\left(\frac{\partial w}{\partial x} - \phi\right)\right] = 0. \tag{16}$$

4. DYNAMIC STIFFNESS MATRICES

According to Liu and Lin [16] and Eisenberger [17, 18], dynamic stiffness matrices relate amplitudes of sinusoidal varying forces at the ends of a member to corresponding displacement amplitudes. Let the harmonic response of vibration for the Timoshenko beam be

$$u(x,t) = u(x)\sin\omega t, \tag{17}$$

$$w(x,t) = w(x)\sin\omega t, \tag{18}$$

$$\phi(x,t) = \phi(x)\sin\omega t. \tag{19}$$

Introducing a normalized variable $\xi = x/L$ where L denotes the element length, the area $A(x)$ and moment of inertia $I(x)$ of a variable cross-section beam element are written as

$$A(x) = \sum_{i=0}^{m} A_i x^i = a(\xi) = \sum_{i=0}^{m} a_i \xi^i, \tag{20}$$

$$I(x) = \sum_{i=0}^{3m} I_i x^i = P(\xi) = \sum_{i=0}^{3m} p_i \xi^i, \tag{21}$$

where m is the number of terms in the fitting polynomial of the beam. Substituting equations (17)–(21) into equations (14)–(16) yields

$$\omega^2 \rho L^2 a(\xi) u(\xi) + \frac{\mathrm{d}}{\mathrm{d}\xi}\left[a(\xi)\frac{\mathrm{d}u(\xi)}{\mathrm{d}\xi}\right] = 0, \tag{22}$$

$$\omega^2 \rho L a(\xi) w(\xi) + \frac{\mathrm{d}}{\mathrm{d}\xi}\left\{ kGa(\xi)\left[\frac{\mathrm{d}w(\xi)}{\mathrm{d}\xi} - L\phi(\xi)\right]\right\} = 0, \tag{23}$$

$$\omega^2 \rho L^2 P(\xi)\phi(\xi) + \frac{\mathrm{d}}{\mathrm{d}\xi}\left[kEP(\xi)\left(\frac{\mathrm{d}\phi(\xi)}{\mathrm{d}\xi}\right)\right] + kGLa(\xi)\left[\frac{\mathrm{d}w(\xi)}{\mathrm{d}\xi} - L\phi(\xi)\right] = 0. \tag{24}$$

It is assumed that the solutions $u(\xi)$, $w(\xi)$, and $\phi(\xi)$ are expressed in series as

$$u(\xi) = \sum_{i=0}^{\infty} u_i \xi^i, \quad w(\xi) = \sum_{i=0}^{\infty} w_i \xi^i, \quad \text{and} \quad \phi(\xi) = \sum_{i=0}^{\infty} \phi_i \xi^i \tag{25}$$

whose coefficients u_i, w_i and ϕ_i will be determined. $u(\xi)$, $w(\xi)$, and $\phi(\xi)$ become exact solutions as i approaches infinity. The coefficients in the solutions read

$$u_{i+2} = \frac{-1}{(i+1)(i+2)a_0}\left[\omega^2 \rho L^2 \sum_{j=0}^{i} a_j u_{i-j} + \sum_{j=1}^{i} (i-j+1)(i-j+2) E a_k u_{i-j+2} \right.$$

$$\left. + \sum_{j=0}^{i} (j+1)(i-j+1) E a_{j+1} u_{i-j+1} \right], \tag{26}$$

$$w_{i+2} = \frac{-1}{(i+1)(i+2)kGa_0}\left[\omega^2\rho L^2 \sum_{j=0}^{i} a_j w_{i-j} + kG \sum_{j=1}^{i} (i-j+1)(i-j+2)a_j w_{i-j+2}\right.$$

$$+ kG \sum_{j=0}^{i} (j+1)(i-j+1)a_{j+1} w_{i-j+1} - kGL \sum_{j=0}^{i} (i-j+1)a_j \phi_{i-j+1}$$

$$\left. - kGL \sum_{j=0}^{i} (j+1)a_{j+1}\phi_{i-j}\right], \tag{27}$$

$$\phi_{i+2} = \frac{-1}{(i+1)(i+2)Ep_0}\left[\omega^2\rho L^2 \sum_{j=0}^{i} p_j \phi_{i-j} + E \sum_{j=0}^{i} (j+1)(i-j+1)p_{j+1}\phi_{i-j+1}\right.$$

$$+ E \sum_{j=1}^{i} (i-j+1)(i-j+2)p_j \phi_{i-j+2}$$

$$+ kGL \sum_{j=0}^{i} (i-j+1)a_j w_{i-j+1}$$

$$\left. - kGL^2 \sum_{j=0}^{i} (i-j)a_j \phi_{i-j}\right]. \tag{28}$$

Hence, all the coefficients of the solutions $u(\xi)$, $w(\xi)$, and $\phi(\xi)$ are obtained except the first two, which will be found by applying boundary conditions. The terms in the stiffness matrix are defined as the forces at both ends of the beam due to unit displacement at each of the degrees of freedom. Therefore, there will be six unit displacement boundary conditions given by

$$1)\ u_1(0) = 1, \qquad u_1(1) = w_1(0) = w_1(1) = \phi_1(0) = \phi_1(1) = 0, \tag{29}$$

$$2)\ w_2(0) = 1, \qquad u_2(0) = u_2(1) = w_2(1) = \phi_2(0) = \phi_2(1) = 0, \tag{30}$$

$$3)\ \phi_3(0) = 1, \qquad u_3(0) = u_3(1) = w_3(0) = w_3(1) = \phi_3(1) = 0, \tag{31}$$

$$4)\ u_4(1) = 1, \qquad u_4(0) = w_4(0) = w_4(1) = \phi_4(0) = \phi_4(1) = 0, \tag{32}$$

$$5)\ w_5(1) = 1, \qquad u_5(0) = u_5(1) = w_5(0) = \phi_5(0) = \phi_5(1) = 0, \tag{33}$$

$$6)\ \phi_6(1) = 1, \qquad u_6(0) = u_6(1) = w_6(0) = w_6(1) = \phi_6(0) = 0. \tag{34}$$

Using the boundary conditions in equations (29)–(34) and the force–strain relations in equations (11)–(13), longitudinal force $B(\xi)$, shear force $V(\xi)$, and bending moment $M(\xi)$ due to unit displacements at both ends of the beam, $\xi = 0$ and 1, become

$$B(0) = -\frac{Ea(\xi)}{L}\frac{\partial u(\xi)}{\partial \xi}\bigg|_{\xi=0} = -\frac{Ea(0)}{L}u_{1,i}, \tag{35}$$

$$V(0) = kGa(\xi)\left[\frac{1}{L}\frac{\partial w(\xi)}{\partial \xi} - \phi(\xi)\right]\Bigg|_{\xi=0}$$

$$= kGa(0)\left[\frac{w_{1,i}}{L} - \phi_{0,i}\right], \tag{36}$$

$$M(0) = -\frac{EP(\xi)}{L}\frac{\partial \phi(\xi)}{\partial \xi}\Bigg|_{\xi=0} = -\frac{EP(0)}{L}\phi_{1,i}, \tag{37}$$

$$B(1) = -\frac{Ea(\xi)}{L}\frac{\partial u}{\partial \xi}\Bigg|_{\xi=0} = \frac{Ea(1)}{L}\sum_{j=0}^{\infty} ju_{j,i}, \tag{38}$$

$$V(1) = -kGa(\xi)\left[\frac{1}{L}\frac{\partial w(\xi)}{\partial \xi} - \phi(\xi)\right]\Bigg|_{\xi=1}$$

$$= -kGa(1)\left[\frac{1}{L}\sum_{j=0}^{\infty} jw_{j,i} - \sum_{j=0}^{\infty}\phi_{j,i}\right], \tag{39}$$

$$M(1) = \frac{EP(\xi)}{L}\frac{\partial \phi(\xi)}{\partial \xi}\Bigg|_{\xi=1} = \frac{EP(1)}{L}\sum_{j=0}^{\infty} j\phi_{j,i}, \tag{40}$$

where $u_{j,i}$, $w_{j,i}$, and $\phi_{j,i}$ denote the jth terms of the ith shape function obtained using the ith, $i = 1$–6, displacement boundary condition in equations (29)–(34) respectively. Finally, using the above formulation for end loading and shape functions, the terms in the dynamic stiffness matrix of the Timoshenko beam vibration are obtained as follows:

(1) For the longitudinal vibration,

$$d(1,i) = -\frac{Ea(0)}{L}u_{1,i}, \tag{41}$$

$$d(4,i) = \frac{Ea(1)}{L}\sum_{j=0}^{\infty} ju_{j,i}, \tag{42}$$

where $u_{j,i}$ denote the jth terms of the ith shape functions and i are 1 and 4 respectively.

(2) For the bending vibration,

$$d(2,i) = kGa(0)\left[\frac{w_{1,i}}{L} - \phi_{0,i}\right], \tag{43}$$

$$d(3,i) = -\frac{EP(0)}{L}\phi_{1,i}, \tag{44}$$

$$d(5,i) = -kGa(1)\left[\frac{1}{L}\sum_{j=0}^{\infty} jw_{j,i} - \sum_{j=0}^{\infty}\phi_{j,i}\right], \tag{45}$$

$$d(6,i) = \frac{EP(1)}{L}\sum_{j=0}^{\infty} j\phi_{j,i}, \tag{46}$$

where $w_{j,i}$ and $\phi_{j,i}$ denote the jth terms of the ith shape functions and $i = 2$, 3, 5, and 6 respectively.

5. GEAR MODELLING AND EXCITATION

As shown in Figure 4(a), a gear tooth is built into its gear blank foundation. In this study, the gear blank effect is accounted for by flexibility coefficients [19] and additional beam elements respectively. Firstly, according to Matusz *et al.* [19] and Cornell [20], treating the gear blank as an elastic half-plane foundation, gear deflection is written as

$$w_V = V/k_{2,2}, \tag{47}$$

$$\theta_V = V/k_{2,3}, \tag{48}$$

$$w_M = M/k_{3,2}, \tag{49}$$

$$\theta_M = M/k_{3,3}, \tag{50}$$

where w_V and θ_V denote translational and rotational displacements due to the shear force V, and w_M and θ_M represent displacements due to the bending moment M. The flexibility coefficients $k_{i,j}$ are written as

$$k_{2,2} = \frac{\pi B_1 E}{2\left[\left(\frac{H}{h'} + \frac{1}{2}\right)\ln\left(\frac{H}{h'} + \frac{1}{2}\right) - \left(\frac{H}{h'} - \frac{1}{2}\right)\ln\left(\frac{H}{h'} - \frac{1}{2}\right) + \frac{1}{2}\right]}, \tag{51}$$

$$k_{3,2} = k_{2,3} = \frac{EB_1 h'}{(1 - \nu)} \tag{52}$$

and

$$k_{3,3} = \frac{\pi E B_1 h'^2}{16.67}, \tag{53}$$

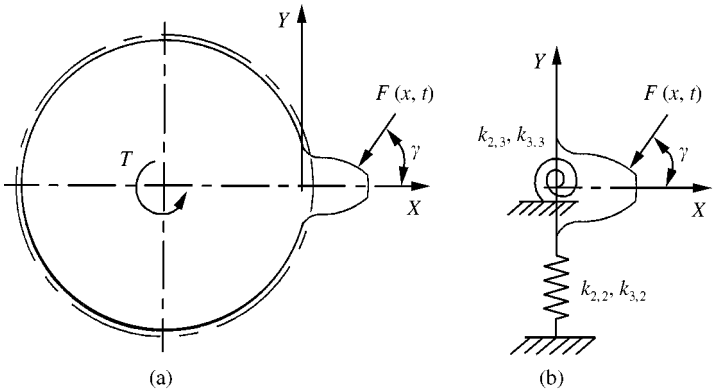

Figure 4. Equivalent dynamic model of gear: (a) shaft-driven torque and meshing force, (b) built-in end boundary conditions.

where H/h' is assumed to be 2·5 [20], $h' = h + 1{\cdot}5r_f$, h is the depth of the beam, and r_f the fillet radius, B_1 the face width of the gear tooth, and v the Poisson's ratio. As a result, the equivalent gear model with boundary conditions is shown in Figure 4(b). For a cantilever beam without the elastic foundation effect, all the flexibility coefficients $k_{i,j}$ approach infinity. The other model uses additional variable cross-section beam elements to represent the gear blank.

In a single-tooth model, a gear meshing force arises from shaft-driven torque. For a given transmitted torque T applied to the gear shaft, the meshing force on the driven gear tooth is shown in Figure 4(a) and assumed as

$$F(x, t) = \frac{T}{r_b n_t}, \tag{54}$$

where $F(x, t)$ is the meshing force and is normal to the involute profile of the gear tooth, T the transmitted torque, r_b the radius of the base circle, and n_t the number of gear teeth that share the meshing force. For a low contact ratio gear system, n_t is one or two. In this study, the shaft-driven torque is assumed to be constant. The x and y components of this force are derived as

$$F_x = F(x, t)\cos\gamma, \tag{55}$$

$$F_y = F(x, t)\sin\gamma, \tag{56}$$

where angle γ is shown in Figure 4. Since the x component is not aligned with the x-axis, its effect is converted to an equivalent moment M_{eq} with its moment center at the origin of the x–y co-ordinate system, depicted in Figure 4(b), i.e.,

$$M_{eq} = F_x(x, t)y. \tag{57}$$

Since the meshing point varies with time, the force components change during gear meshing.

This paper further deals with a tooth pair with two mating gears as shown in Figure 5. The tooth pair is driven by a shaft-driven torque. Gear blanks are not simplified to be lumped stiffness. Instead, each gear blank consists of two variable cross-section beam elements. Two gear teeth are connected by a non-linear contact stiffness at the meshing points. The meshing points which vary with time are recalculated for each numerical calculation step. According to Weber [21], the non-linear contact stiffness is obtained using the Hertz contact stress and compression between the meshing point and the tooth centerline. While the tooth pair is subjected to a contact force F, its local deformation Y_L can be expressed as

$$Y_L = F/k_H, \tag{58}$$

where k_H is the non-linear contact stiffness given by [21]

$$k_H = \frac{B_1}{4}\frac{\pi E}{1 - v^2}\left\{\ln\left(\frac{2\sqrt{h_1 h_2}}{b} - \left[\frac{v}{2(1 - v)}\right]\right\}^{-1} \tag{59}$$

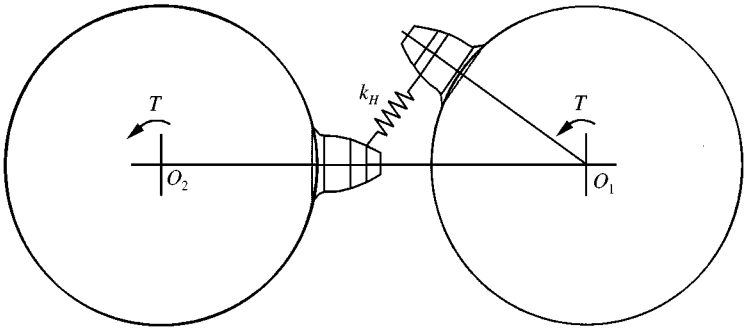

Figure 5. A tooth pair with a contact stiffness.

and

$$b = \left[\frac{2F}{\pi B_1}\left(\frac{1-v^2}{E}\right)\frac{r_1 r_2}{r_1 + r_2}\right]^{1/2}, \tag{60}$$

where b is the Hertz half contact length, h_1 and h_2 are distances from contact points along the line of contact to the center of the contact teeth, and r_1 and r_2 are curvature radii of tooth profiles for gears 1 and 2 respectively. At the first time, F is calculated using equation (54). Subsequently, F is obtained from the calculation results in the previous step. The non-linear contact stiffness k_H is appended to the dynamic stiffness matrices of the mating teeth.

6. MODAL ANALYSIS

Relating a stiffness and force in a harmonically vibratory system, the dynamic stiffness matrix $\mathbf{D}(\omega)$ composed of elements $d(i, j)$ that have been formulated in equations (41)–(46) is defined by [22]

$$\mathbf{D}(\omega)\psi = \mathbf{F}_h, \tag{61}$$

where ψ is an eigenvector and $\mathbf{F}_h$ represents an external harmonic force vector. Since a system consists of several variable cross-section members, the dynamic stiffness matrix $\mathbf{D}(\omega)$ is assembled over all the subsystems as traditionally done in finite element analysis. In this work, the gear tooth is divided into four beam elements.

The natural frequencies of a vibratory system are the values when equation (61) has non-trivial homogeneous solutions ψ, i.e.,

$$\det \mathbf{D}(\omega) = 0. \tag{62}$$

This determinant is calculated by incrementally increasing ω until sign changes are observed. A bisection numerical procedure is performed to speed up convergence of the natural frequencies to a desired accuracy.

For vibration analysis of linear systems undergoing forced harmonic oscillation, one has

$$\mathbf{D}(\omega) = \mathbf{K} - \omega^2\mathbf{M}, \tag{63}$$

where **K** and **M** are stiffness and mass matrices respectively. From Leung's theorem [22], the mass and stiffness matrices are derived as

$$\mathbf{M} = -\frac{\partial \mathbf{D}(\omega)}{\partial \omega^2}, \tag{64}$$

$$\mathbf{K} = \mathbf{D}(\omega) - \omega^2 \frac{\partial \mathbf{D}(\omega)}{\partial \omega^2}. \tag{65}$$

In this work, a displacement response vector **q** is defined as

$$\mathbf{q} = [u_1 \;\; w_1 \;\; \phi_1 \cdots u_n \;\; w_n \;\; \phi_n]^{\mathrm{T}}, \tag{66}$$

where n is the number of nodes on the gear tooth. Further, a componental response vector $\mathbf{q}_i$ is defined as a component of **q** due to the ith mode with a natural frequency ω_i. Therefore,

$$\mathbf{q} = \sum_{i=1}^{N} \mathbf{q}_i, \tag{67}$$

where N is the number of modes taken into account for a desired accuracy of the response. Using $\mathbf{M}_i$ and $\mathbf{K}_i$ in terms of the natural frequency ω_i obtained by equations (64) and (65), excitation force **F**, and initial conditions, the displacement $\mathbf{q}_i$ can be solved from

$$\mathbf{M}_i \ddot{\mathbf{q}}_i + \mathbf{K}_i \mathbf{q}_i = \mathbf{F}. \tag{68}$$

The modal response is obtained by performing the Runge–Kutta method for equation (68). Further, the free and forced responses **q** at nodes are obtained by superimposing all the displacement responses $\mathbf{q}_i$. Finally, based on these nodal displacements, the strains and stresses at an arbitrary point in the tooth can be calculated.

7. NUMERICAL RESULTS AND DISCUSSION

Based on the flowchart in Figure 6, a computer program is written to calculate (1) the x and y co-ordinates of points along the involute profile and fillet of a spur gear, (2) the gear meshing point used for elements dividing and force imposing node, (3) normalized polynomials which fit the gear, (4) dynamic stiffness matrices of the beam and its natural frequencies, (5) meshing force and components along the tooth profile, and (6) dynamic responses and stresses of the gear tooth.

7.1. EXAMPLE 1

A thin spur gear tooth is subjected to a moving meshing force, the data of which is shown in Table 1. Both stiffness and inertia matrices of the gear tooth for the present model during gear meshing are time- and position-varying. To validate the proposed method, dynamic stresses at a tooth fillet are compared with results by the finite element method [13]. Firstly, the gear rotates at a low speed of 748 rpm. The gear blank effect is incorporated using the flexibility coefficients. Natural frequencies of the first three modes are 150 230, 409 070, and 459 070 rad/s. In this work, the tooth displacements and stresses are calculated. To account

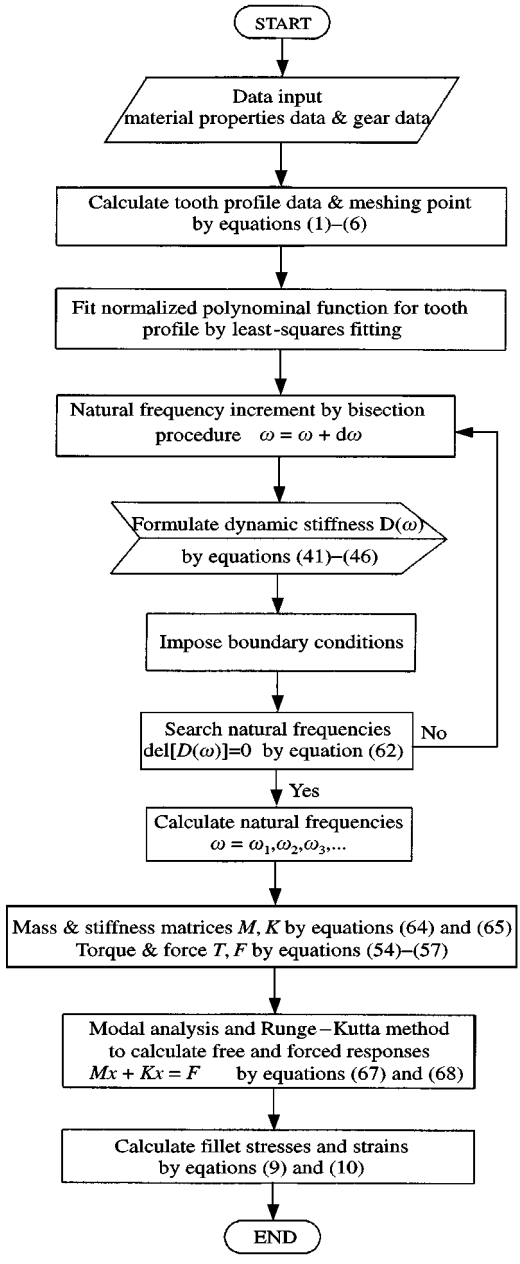

Figure 6. Flowchart of gear tooth vibration analysis.

for the meshing process, a meshing force of 245·25 N per unit gear face width, induced by a shaft-driving torque 230·46 N m, moves along the tooth profile from the tooth tip to the root. Damping ratios are assumed as $\varsigma = 0{\cdot}004$ and 0·02. Figure 7 shows the tip transverse displacement and the fillet stress for damping ratio $\varsigma = 0{\cdot}004$ during tooth meshing. These values are obtained by superimposing responses of the first three modes. Besides, Figure 8 depicts superimposed results for damping ratio $\varsigma = 0{\cdot}02$. Concerning the results in Figures 7(a) and 8(a), the initial meshing causes a large displacement at the tooth tip, followed by

TABLE 1

Gear tooth parameters

Parameter	Value
Pressure angle	20°
Module (M)	10 mm
Addendum	1 M
Dedendum	1·25 M
Teeth number	20
Face width	2 M
Rotation speed	78·25 rad/s

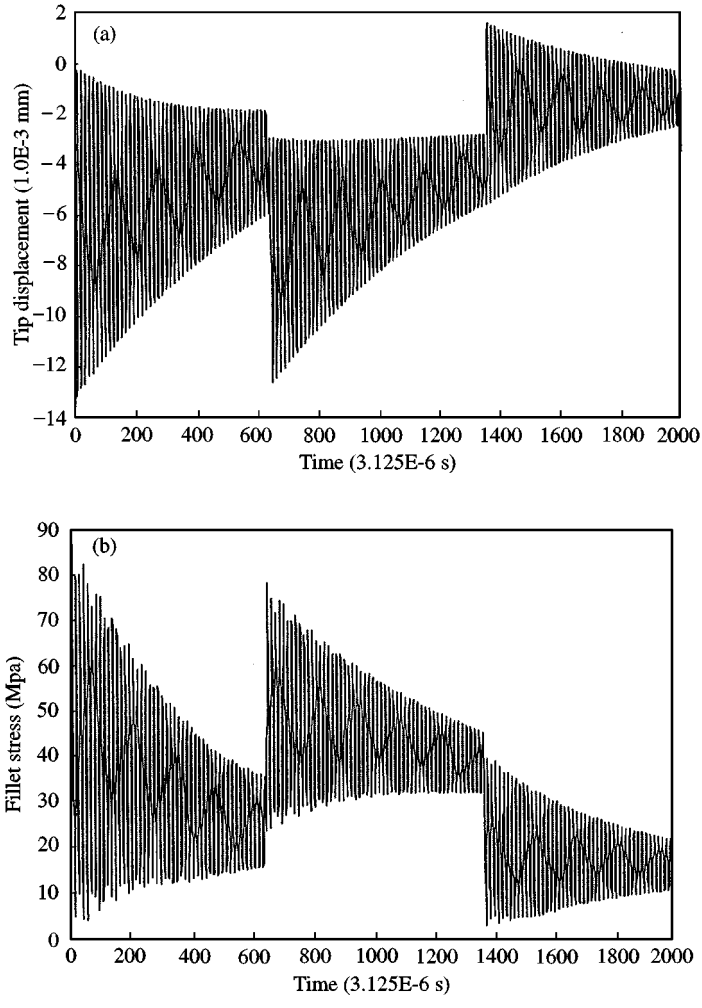

Figure 7. Dynamic displacement and stress for damping ratio $\zeta = 0{\cdot}004$ at 748 rpm: (a) tip displacement; (b) fillet stress.

a sinusoidal displacement with an exponential decay. This decaying tendency is maintained until the number of contact teeth changes from two to one, at the instant $640 \times 3{\cdot}125\text{E} - 6\,\text{s} = 0{\cdot}002\,\text{s}$, where the amplitude exhibits a sudden jump. However, this amplitude is still smaller than that at initial contact, since the bending moment caused by

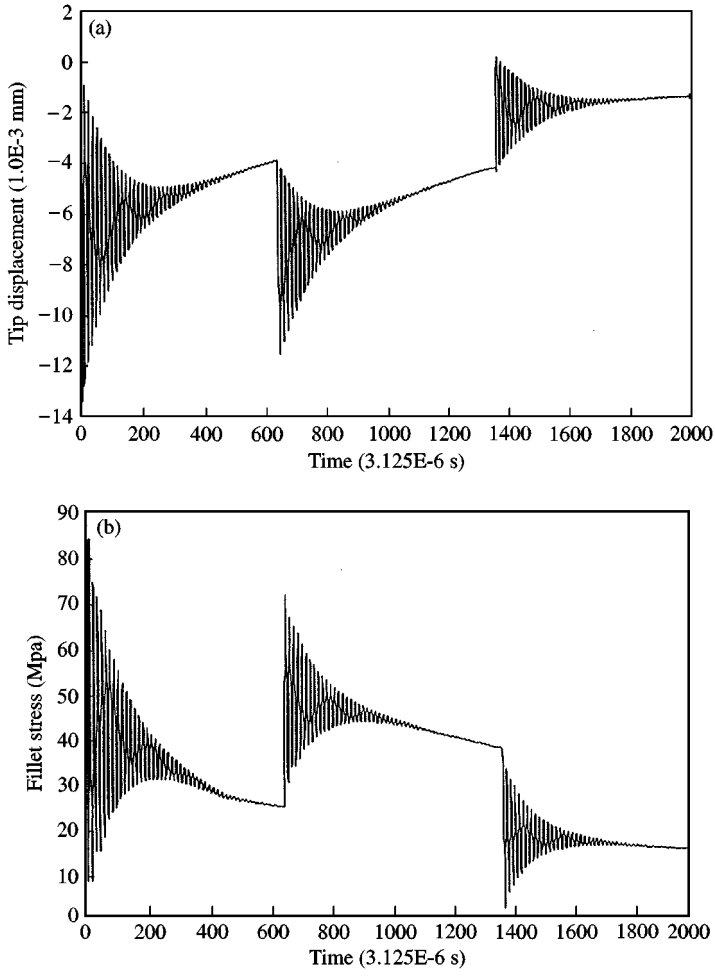

Figure 8. Dynamic displacement and stress for damping ratio $\zeta = 0{\cdot}02$ at 748 rpm: (a) tip displacement; (b) fillet stress.

the meshing force when the teeth contact at the tip is larger than at elsewhere. Moreover, stiffness at the tooth tip is smaller than elsewhere due to the smallest thickness at the tip. Finally, as soon as the second amplitude jump appears, the tooth undergoes vibration with smaller amplitudes, since the meshing point is closer to the root and the contact teeth number on this gear becomes two again. Besides, comparing Figures 7(a) and 8(a) shows that vibratory displacement for damping ratio $\varsigma = 0{\cdot}004$ decays slower than that for $\varsigma = 0{\cdot}02$. However, the damping ratio does not significantly affect their maximum amplitudes, which are observed as 0·0131 and 0·0127 mm for $\varsigma = 0{\cdot}004$ and 0·02 respectively. From vibratory displacements, stresses at the fillet are calculated and shown in Figures 7(b) and 8(b). The results agree well with those in the literature [13]. Additionally, for the gear rotating at a much higher speed of 4000 rpm, the responses of the tooth are depicted in Figure 9, which have shorter meshing periods and fewer vibratory cycles than those in Figure 7. The maximum values of the tip displacement and fillet stress depicted in Figure 9 are larger than those in Figure 7.

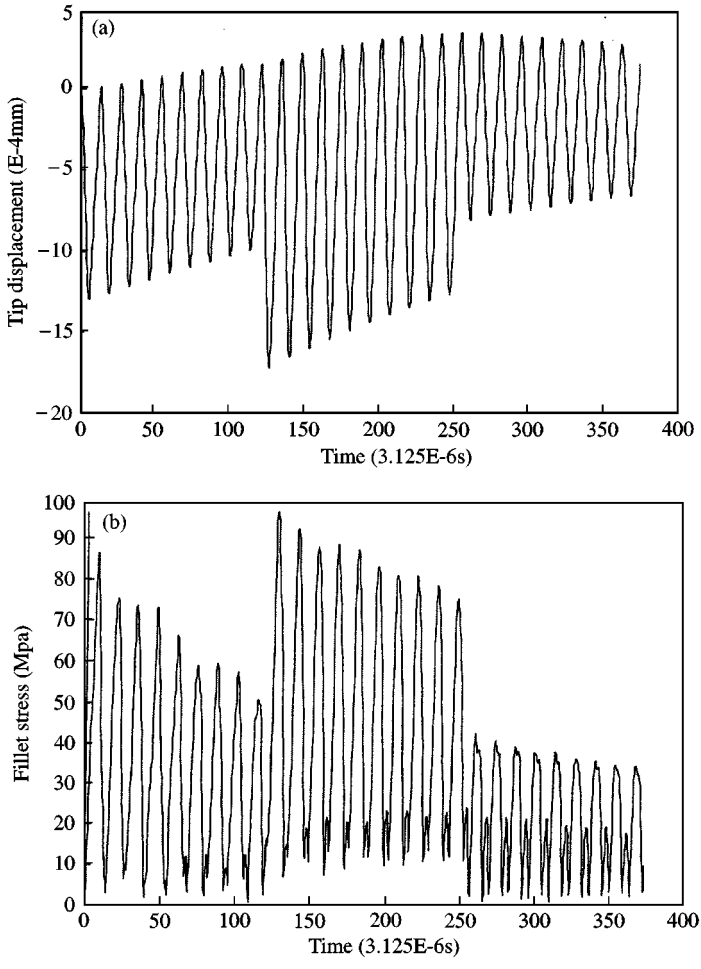

Figure 9. Dynamic displacement and stress for damping ratio $\zeta = 0{\cdot}004$ at 4000 rpm: (a) tip displacement; (b) fillet stress.

7.2. EXAMPLE 2

The gear blank model is incorporated using two variable cross-section beam elements. Only the response for the damping ratio $\varsigma = 0{\cdot}004$ is calculated. The first seven natural frequencies are calculated as 51 930, 87 358, 118 713, 138 911, 169 047, 179 880, and 216 357 rad/s respectively. Figure 10(a) shows the fillet stress obtained by superimposing responses of these seven natural modes. Their peak values are a little smaller than, but close to, the result depicted in Figure 7(a). Responses due to individual modes are given in Figures 10(b)–10(d). As shown in Figures 10(b) and 10(c), the two lowest modes contribute little to the superimposed result in Figure 10(a), and so do the third and fourth modes. However, as depicted in Figure 10(d), the fifth mode of 169 047 rad/s dominates the response and it is close to the first natural frequency obtained by the former model. The sixth and seventh modes are high-frequency modes, and so result in less contribution again.

The first seven natural frequencies of the gear obtained by both models are compared in Figure 11. When dynamic performance of the entire gear is desired, the modal

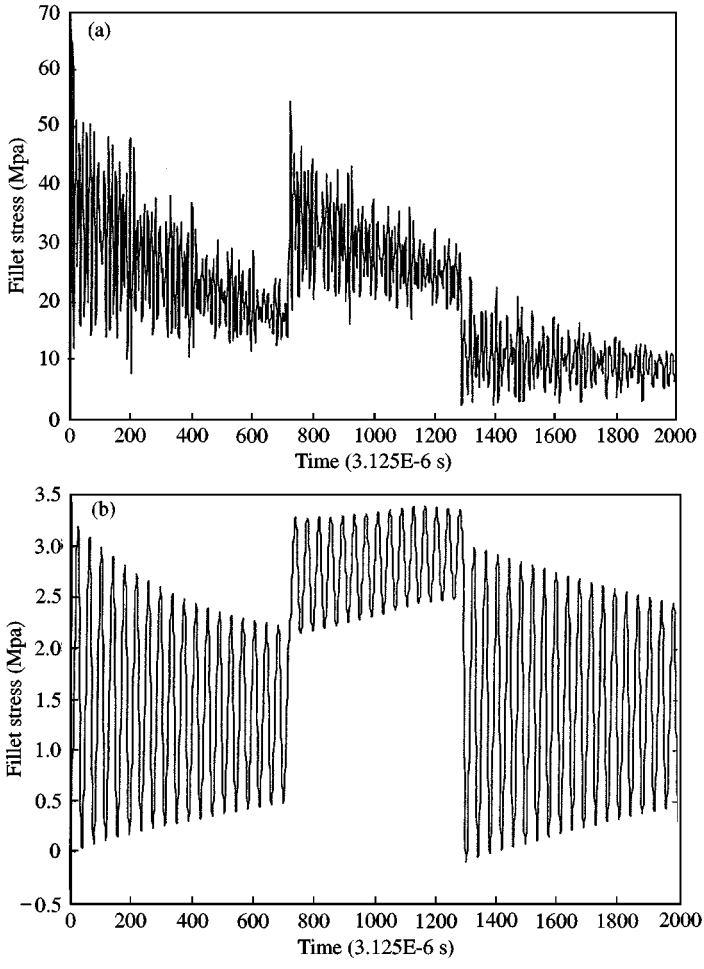

Figure 10. Superimposed fillet stress for damping ratio $\zeta = 0{\cdot}004$: (a) superimposed result, (b)–(d) results due to some individual natural modes.

characteristics of the gear blank has to be taken into account, since it will generate lower natural frequencies.

However, these frequency modes do not critically affect tooth dynamic behavior. By contrast, the higher modes induced by the tooth part dominates when only tooth dynamics is concerned. Further, the superimposed responses modelled by the flexibility coefficients and gear blank are close. Therefore, the model employing the flexibility coefficients is validated. Further, when the dynamic response of a tooth is measured, the measurement bandwidth has to be high enough to contain higher modes that are caused by the tooth part.

7.3. EXAMPLE 3

This example calculates the fillet strain of a tooth pair on two mating identical gears with standard tooth profiles. The dynamic fillet strain of the driven gear is compared with the empirical result presented by Oswald and Townsend [23]. The gears rotate at 4000 rpm

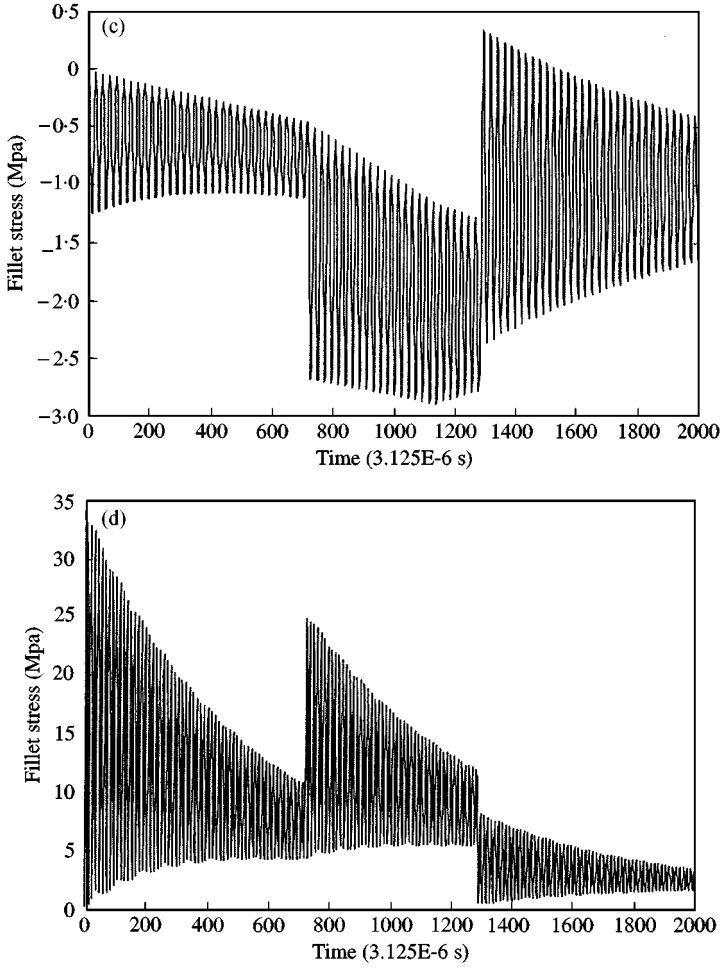

Figure 10. Continued

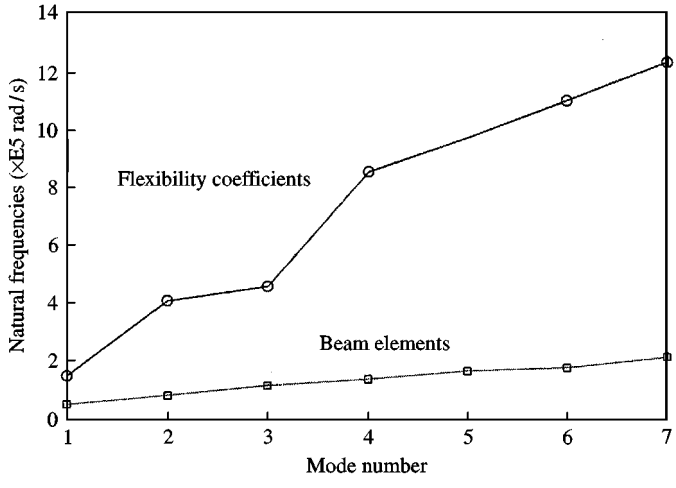

Figure 11. Frequencies distribution of gear tooth using different models for gear blank.

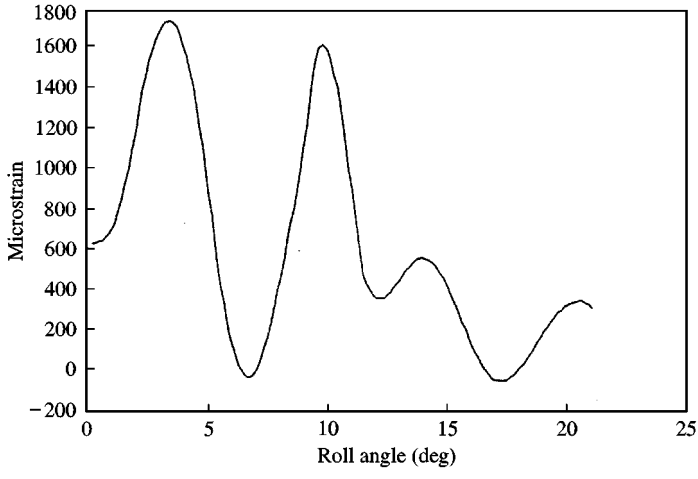

Figure 12. Fillet strain of driven gear.

with a driving torque 102 N m. The fillet microstrain of the driven gear is depicted in Figure 12. Two large peak values occurred. One peak of value 2076 is generated at the instant of 3·28° due to meshing at the tooth tip of the driven gear. The other occurs at the instant of 9·60°, since the number of meshing tooth pair changes from two to one. After that, the strain becomes smaller, since not only the meshing point approaches a tooth root on the driven gear, but the number of meshing tooth pairs also changes back to two. The present result is similar to empirical results in the literature [23].

8. CONCLUSIONS

A dynamic stiffness method based on equations of motion for a Timoshenko beam model has been developed to simulate spur gear dynamics during meshing. In this work, rather than the finite element method, the dynamic stiffness method is used to calculate the dynamic response of a gear tooth subject to meshing force. Instead of discrete models, this method deals with time-varying mass and stiffness matrices and meshing force due to the movement of meshing points that are crucial factors causing gears vibration and noise. When dynamic performance of the entire gear is desired, the gear blank has to be taken into account since it generates lower natural frequencies. However, the gear blank does not critically affect the peak values of the fillet stress and tip displacement. By contrast, the higher modes induced by the tooth part will dominate. Dynamics of a tooth pair represented by two beams connected by a non-linear contact stiffness has also been investigated. Since the gear tooth is modelled by variable cross-section Timoshenko beams with curve profiles, variation of gear design parameters, and contact ratio on gear performance can be further investigated to facilitate gear design.

ACKNOWLEDGMENT

This work was sponsored by National Science Council, Republic of China, under grant No. NSC89-2212-E009-048.

REFERENCES

1. H. N. OZGUVEN and D. R. HOUSER 1988 *Journal of Sound and Vibration* **121**, 383–411. Mathematical models used in gear dynamics—a review.
2. F. CUNLIFFE, J. D. SMITH and D. B. WELBOURN 1974 *ASME Journal of Engineering for Industry* **96**, 578–584. Dynamic tooth loads in epicyclic gears.
3. M. BOTMAN 1976 *ASME Journal of Engineering for Industry* **98**, 811–815. Epicyclic gear vibrations.
4. D. L. SEAGER 1975 *Journal of Mechanical Engineering Science* **17**, 293–298. Conditions for the neutralization of excitation by the teeth in epicyclic gearing.
5. T. HIDAKA, Y. TERAUCHI and K. NAGAMURA 1979 *Bulletin of the JSME* **22**, 1026–1033. Dynamic behavior of planetary gear-6th report, displacement of sun gear and ring gear.
6. A. KAHRAMAN 1994 *ASME Journal of Mechanical Design* **116**, 713–720. Planetary gear train dynamics.
7. P. VELEX and L. FLAMAND 1996 *ASME Journal of Mechanical Design* **118**, 7–14. Dynamic response of planetary gear trains to mesh parametic excitations.
8. K. NAGAYA 1979 *Journal Acoustical Society of America* **66**, 794–800. Approximate dynamic analysis of Timoshenko beams and its application to tapered beams.
9. K. NAGAYA 1981 *ASME Journal of Mechanical Design* **103**, 357–363. Effects of moving speeds of dynamic loads on the deflections of gear teeth.
10. K. UMEZAWA, T. SATO and J. ISHIKAWA 1984 *Bulletin of the JSME* **27,** 102–109. Simulation on rotational vibration of spur gears.
11. K. UMEZAWA 1972 *Bulletin of the JSME* **90**, 1632–1639. The meshing test on helical gears under load transmission-1st report, the approximate formula for deflections of gear tooth.
12. F. M. AMIROUCHE, G. C. TAJIRI and M. J. VALCO 1995 *International Journal for Numerical Methods in Engineering* **39**, 2073–2094. Mathematical model of a time and position variant external load on a gear tooth using the modified Timoshenko beam equation.
13. S. VIJAYARANGAN and N. GANESAN 1993 *Journal of Sound and Vibration* **162**, 185–189. A study of dynamic stresses in a spur gear under a moving line load and impact load conditions by a three-dimension finite element method.
14. F. L. LITVIN 1994 *Gear Geometry and Applied Theory*. London: Prentice-Hall.
15. C. L. DYM and I. H. SHAMES 1973 *Solid Mechanics—a Variational Approach*. New York: McGraw-Hill.
16. T. S. LIU and J. C. LIN 1993 *ASME Journal of Vibration and Acoustics* **115**, 468–476. Forced vibration of flexible body system: a dynamic stiffness method.
17. M. EISENBERGER 1990 *AIAA Journal* **28**, 1105–1109. Exact static and dynamic stiffness matrices for variable cross section members.
18. M. EISENBERGER 1995 *Communications in Numerical Methods in Engineering* **11**, 507–513. Dynamic stiffness matrix for variable cross-section Timoshenko beams.
19. J. M. MATUSZ, W. J. O'DONNEL and R. J. ERDLAC 1969 *ASME Journal of Engineering for Industry* **91**, 607–614. Local flexibility coefficients for the built-in ends of beams and plates.
20. R. W. CORNELL 1981 *ASME Journal of Mechanical Design* **103**, 447–459. Compliance and stress sensitivity of spur gear teeth.
21. C. WEBER 1949 *Sponsored Research* (*Germany*) *Department of Scientific and Industrial Research, Report No*. 3. The deformation of loaded gears and the effect on their load-carrying capacity.
22. T. H. RICHARDS and A. Y. T. LEUNG 1977 *Journal of Sound and Vibration* **55**, 363–376. An accurate method in structural vibrating analysis.
23. F. B. OSWALD and D. P. TOWNSEND 1996 *Gear Technology* **13**, 20–24. Tooth modification and spur gear tooth strain.